Submitted to the
International Europhysics Conference on High Energy Physics
Aachen, Germany, July 17 – July 23, 2003

Abstract: 516 **Parallel Session: HQCD, HP**

Measurement of Strange Particle Production in Deep Inelastic $e^+p \to e^+X$ Scattering at HERA

ZEUS Collaboration

Abstract

A measurement of inclusive K^0_S, Λ and $\overline{\Lambda}$ production in deep inelastic ep scattering at HERA is presented for an integrated luminosity of 60 pb^{-1}. Kinematic distributions for K^0_S, Λ, $\overline{\Lambda}$ production and $(\Lambda + \overline{\Lambda})/K^0_S$, $\Lambda/\overline{\Lambda}$ ratios have been measured in the laboratory and in the Breit frames for $50 < Q2 < 500$ GeV^2, and compared to Monte Carlo models. The measurement of the ratios agrees with models based on the Lund string fragmentation model. However, the dependence of the K^0_S production cross section on the scaled momentum fraction $x_p = 2 \cdot p^{\mathrm{Breit}}/Q$ in the target region of the Breit frame is not reproduced by the models.

1 Introduction

This paper reports a study of K_S^0–meson and Λ–baryon production in neutral current e^+p deep inelastic scattering (DIS) and explores its sensitivity to strange quark production in fragmentation as implemented in Monte Carlo (MC) simulations.

One successful fragmentation model is the Lund string model [1], which uses probabilities P_s, P_u and P_d for creating s, u and d quarks, respectively, in the colour field during the fragmentation process. Since u and d quarks have low mass compared to the strange quark, it is assumed that $P_u = P_d$. The higher mass of the s quark leads to a suppression that is quantified by the strangeness suppression factor, $\lambda_s = P_s/P_u$.

The value, $\lambda_s = 0.3$, found in e^+e^- annihilation [2], is normally used as the default value in the model. However, there are recent indications that a larger value, $\lambda_s \approx 0.4$, may be needed [3], or that a single value cannot accommodate all the SLD strangeness–production data [4]. When using the same hadronisation model in e^+p scattering, the measured K_S^0, Λ and ϕ rates in DIS

[5] and photoproduction [6] indicate the need for a smaller value, $\lambda_s \approx 0.2$. For Λ production, in the Lund model, there is also an extra suppression of strange diquark production, $\delta = \frac{P(us)/P(ud)}{P(s)/P(d)}$, which has not been varied for this study. A detailed understanding of strangeness production and fragmentation will be a necessary requirement in the precise measurement of the strange sea and the strange structure function, F_2^s.

2 Experimental setup

The data analysed for this study were taken during the 1999 to 2000 running period. During this period, the positron and proton beam energies were 27.5 GeV and 920 GeV, respectively, corresponding to an integrated luminosity of 60 pb^{-1}.

The ZEUS detector is described in detail elsewhere [7]. Of particular importance in the present study are the central tracking detector and the calorimeter.

The central tracking detector (CTD) [8] is a cylindrical drift chamber with nine superlayers covering the polar–angle[1] region $15° < \theta < 164°$ and the radial range 18.2–79.4 cm. Each superlayer consists of eight sense–wire layers which are organised either of wires parallel (axial) to the beam axis or of wires inclined at a small stereo angle to allow accurate

[1] The ZEUS coordinate system is a right-handed Cartesian system, with the Z axis pointing in the proton beam direction, referred to as the “forward direction”, and the X axis pointing left towards the centre of HERA. The coordinate origin is at the nominal interaction point.

z reconstruction. The transverse–momentum resolution for charged tracks traversing all CTD layers is $\sigma(p_T)/p_T = 0.0058 p_T \oplus 0.0065 \oplus 0.0014/p_T$, with p_T in GeV.

The CTD is surrounded by the uranium–scintillator, CAL [9], which is divided into three parts: forward, barrel and rear. The calorimeter is longitudinally segmented into electromagnetic and

hadronic sections. The energy resolution of the calorimeter under test–beam conditions is $\sigma_E/E = 0.18/\sqrt{E}$ for electrons and $\sigma_E/E = 0.35/\sqrt{E}$ for hadrons with E in GeV.

3 Kinematic reconstruction and event selection

For the DIS selection, the scattered–positron candidates were identified from the energy deposits in the CAL [10]. The kinematic variables are photon virtuality, $Q^2 = -(k-k')^2$, the Bjorken scaling variable, $x = Q^2/(2p \cdot q)$, and the inelasticity, $y = p \cdot q / p \cdot k$. They were reconstructed using the following three methods:

- the electron method (denoted by the subscript e) which uses measurements of the energy and angle of the scattered positron;
- the double angle (DA) method [11, 12] which relies on the angles of the scattered positron and of the hadronic energy flow;
- the Jacquet–Blondel (JB) method [13], based on measurements of the hadronic system.

The DIS event selection was based on the following requirements:

- $E_{e'} > 10\,\text{GeV}$, where $E_{e'}$ is the energy of the scattered positron in the calorimeter after the correction by the presampler [14, 15];
- $50 < Q^2_{\text{DA}} < 500\,\text{GeV}^2$, to restrict the measurement to a range with sufficient statistics for differential cross sections; this corresponds to an x range of $3 \cdot 10^{-4} < x < 10^{-1}$;
- $40 < \delta < 60\,\text{GeV}$, where $\delta = \sum E_i(1-\cos\theta_i)$. E_i is the energy of the ith cell, the smallest subdivision of the CAL, and θ_i is its angle. The sum runs over all cells. This cut further reduces the background from photoproduction and events with large inital–state radiation;
- $y_e < 0.8$, to remove events with fake scattered positron candidates;
- $y_{\text{JB}} > 0.04$, to improve the accuracy of the DA reconstruction;
- a primary vertex position, from the primary vertex fit, in the range $|Z_{\text{vertex}}| < 50\,\text{cm}$, to reduce background events from non–ep interactions;
- the impact point (X,Y) of the scattered positron in the calorimeter must be outside a radius $\sqrt{X^2+Y^2} > 36\,\text{cm}$, to avoid the rear beam hole in the CAL.

The values $Q^2_{\rm DA}$ and $x_{\rm DA}$ were used as the estimates of Q^2

and x since the DA method has the best resolution at the relatively high Q^2 values of this data set.

4 Selection of strange particle candidates

Charged tracks measured by the CTD were selected. Tracks were required to pass through at least three CTD superlayers and to have transverse momenta, $p_T > 150\,{\rm MeV}$, and pseudorapidity in the laboratory frame, $|\eta| < 1.75$, restricting the study to a region where CTD track acceptance and resolution are high. Long lived neutral strange hadrons decaying to two charged particles are identified by selecting pairs of oppositely charged tracks, fitted to a displaced secondary vertex. All pairs of oppositely charged tracks were combined to form K^0_S and Λ candidates.[2]

4.1 Selection of K^0_S candidates

The K^0_S's were identified by their charged decay mode $K^0_S \rightarrow \pi^+\pi^-$. Both the tracks were assigned the mass of the charged pion and the invariant mass, $M(\pi^+\pi^-)$, of each track pair was calculated. The K^0_S candidates were selected using the following requirements:

- $0.45 < M(\pi^+\pi^-) < 0.55\,{\rm GeV}$;
- $M(p\pi) > 1.12\,{\rm GeV}$ to eliminate Λ contamination of the K^0_S signal, where the mass of the proton is assigned to the track with higher momentum and the mass of the charged pion to the second track;
- $0.5 < p^K_T < 5.0\,{\rm GeV}$ and $|\eta^K| < 1.5$, where p^K_T is the transverse momentum and η^K is the pseudorapidity of the K^0_S in the laboratory frame.

Figure 1a shows the fitted invariant–mass distribution of the K^0_S candidates. The fit gives a peak position of $m_{K^0_S} = 497.95 \pm 0.03\,{\rm MeV}$. No systematic uncertainties on the mass have been evaluated.

The number of K^0_S candidates, in the mass range $0.484 < M(\pi^+\pi^-) < 0.510\,{\rm GeV}$, is 48514 ± 234.

[2] In this paper, the nominal Λ sample includes $\overline{\Lambda}$ except where the explicit comparisons of Λ to $\overline{\Lambda}$ production are made.

4.2 Selection of Λ candidates

The Λ candidates were identified by their charged decay mode $\Lambda \to p\pi^-$. For the Λ reconstruction, of the two tracks, the track with the higher momentum was assigned the mass of the proton while the other was assigned the mass of the charged pion. The events with Λ candidates were selected using the following requirements:

- $1.1 < M(p\pi) < 1.13\,\mathrm{GeV}$;
- $0.5 < p_T^\Lambda < 5.0\,\mathrm{GeV}$ and $|\eta^\Lambda| < 1.5$, where p_T^Λ is the transverse momentum and η^Λ is the pseudorapidity of the Λ in the laboratory frame.

Figure 1b shows the fitted invariant–mass distribution for Λ candidates. The fit gives a peak position of $m_\Lambda = 1116.22 \pm 0.02\,\mathrm{MeV}$. No systematic uncertainties on the mass have been evaluated. The numbers of Λ, $\overline{\Lambda}$ and $\Lambda + \overline{\Lambda}$ candidates, in the mass range $1.1126 < M(p\pi) < 1.1198\,\mathrm{GeV}$, from the fit, are 4354 ± 85, 4029 ± 81 and 8351 ± 116, respectively.

5 Event simulation

The measured cross sections were compared to various leading–logarithmic Monte Carlo models which include a QCD parton–cascade followed by subsequent fragmentation to hadrons. Events were generated with HERWIG 6.1 [16] and ARIADNE 4.07 [17]. HERWIG uses a standard DGLAP evolution to simulate the QCD parton shower, whereas ARIADNE uses the colour–dipole–model (CDM) [18]. In both cases, the default parameters were used and the parton density functions were taken from the CTEQ5D set [19]. The hadronisation in ARIADNE is simulated using the Lund string model as implemented in JETSET 7.4 [20], whereas the hadronisation stage in HERWIG is described by a cluster fragmentation model [21].

The acceptance was calculated using ARIADNE, interfaced with HERACLES 4.5.2 using the DJANGOH [22] program in order to incorporate first–order electroweak corrections. The generated events were then passed through a full simulation of the detector using GEANT 3.13 and processed with the same reconstruction program as used for the data. The same selection cuts used for the data were applied to the detector–level MC samples.

6 Definition of cross sections and systematic uncertainties

The K_S^0 and Λ cross sections were measured in the kinematic region $50 < Q^2 < 500\,\mathrm{GeV}^2$, $3 \cdot 10^{-4} < x < 10^{-1}$, $0.5 < p_T^{K_S^0,\Lambda} < 5\,\mathrm{GeV}$ and $|\eta^{K_S^0,\Lambda}| < 1.5$. The cross sections, as a function of a given observable, Y, were determined using

$$\frac{d\sigma}{dY} = \frac{N}{A \cdot \mathcal{L} \cdot B \cdot \Delta Y},$$

where N is the number of events with a K_S^0 or Λ candidate in a bin of size ΔY, A is the acceptance, evaluated using the MC, which takes into account migrations, efficiencies and radiative effects for that bin, and $\mathcal{L}$ is the integrated luminosity. The branching ratios, B, for the decay channel $K_S^0 \to \pi^+\pi^-$ and $\Lambda \to p\pi^-$ were taken as 0.686 ± 0.003 and 0.639 ± 0.005 [23], respectively.

Full systematic errors were calculated for the kinematic selection, strange particle identification and for simulation of the events used for the unfolding. They are shown, added in quadrature with the statistical uncertainty, as the outer error bars in the figures. A normalisation uncertainty due to the luminosity measurement of $\pm 1.7\%$ and the uncertainty in the decay branching ratios were not included.

7 Results

Table 1 gives the total K_S^0 and Λ cross sections for data and MC. Both measured cross sections are lower than those predicted by ARIADNE using $\lambda_s = 0.3$ but higher than for $\lambda_s = 0.2$. The HERWIG predictions underestimate the measured K_S^0 and overestimate the Λ cross sections. The ratio of Λ to K_S^0 total cross sections is reasonably simulated by ARIADNE.

Figure 2 compares the differential K_S^0 (a) and Λ (b) cross sections as functions of p_T with the predictions of ARIADNE and HERWIG. The ARIADNE predictions, shown for $\lambda_s = 0.2$ and $\lambda_s = 0.3$, reproduce the shape of p_T disbtributions reasonably well. For K_S^0, $\lambda_s = 0.2$ is preferred at lower p_T, while for Λ, $\lambda_s = 0.3$ is preferred. The HERWIG distributions, scaled to the area below the data, fail to reproduce the shape for either K_S^0's or Λ's.

The cross section ratios, $d\sigma(\Lambda)/d\sigma(K_S^0)$, as functions of p_T and η, are compared to the ARIADNE and HERWIG models in Fig. 3. The ARIADNE predictions, shown for both $\lambda_s = 0.2$ and $\lambda_s = 0.3$, reproduce the p_T distributions reasonably well, however they do not describe the shape of the η distribution. For the HERWIG predictions, since there is a large disagreement between the measurements and the predicted ratios, the HERWIG ratios have been scaled by 0.28 and 0.32 for p_T and η, respectively, to allow more meaningful shape comparison.

There may be an indication of increased Λ to K^0_S production in the forward region and at low p_T, compared to all three MC models.

Figure 4 shows the differential K^0_S (a,b) and Λ (c,d) cross sections as functions of $p_T^{\rm Breit}$, in the target (left) and current (right) regions of the Breit frame. Fig. 5 shows the cross sections as functions of the scaled momentum, $x_p \equiv 2p/Q$, where p is the absolute value of the momentum of the particle evaluated in the Breit frame, again in the target (left) and current (right) regions. Even after rescaling, HERWIG fails to describe the data for either K^0_S or Λ production, having in general, a p_T distribution which falls too steeply with increasing p_T. The x_p distribution for HERWIG falls more steeply than the data for increasing x_p in the target region, but does not fall steeply enough in the current region. In contrast, the ARIADNE predictions, with both values of strangeness supression factors, describe the $p_T^{\rm Breit}$ and x_p distributions reasonably well in the current region. However, for K^0_S production in the target region, the measurement prefers an increasing λ_s value with increasing x_p, while for Λ production, the measurement agrees better with $\lambda_s = 0.3$.

Figure 6 shows the relative production rate for meson to baryon production, $d\sigma(\Lambda)/d\sigma(K^0_S)$, as functions of $p_T^{\rm Breit}$ (a,b) and x_p (c,d) in the target (left) and current (right) regions of the Breit frame. The dip in the second bin of Fig. 6a, is due to the different $p_T^{\rm Breit}$ distributions of the two particles species and is reproduced by both ARIADNE predictions. As before, to enable more meaningful shape comparisons, the HERWIG predictions have been scaled, this time by 0.31, 0.28, 0.28, 0.45, respectively.

In the current region, the measured ratios are in reasonable agreement with the ARIADNE predictions with $\lambda_s = 0.2$ and $\lambda_s = 0.3$, both for $p_T^{\rm Breit}$ and x_p whereas the scaled HERWIG predictions have a somewhat steeper shape in $p_T^{\rm Breit}$ and x_p than the data. In the target region, the shapes in $p_T^{\rm Breit}$ and x_p are not described particularly well by any of the models.

Figure 7 and shows the ratio $(d\sigma(\Lambda)-d\sigma(\overline{\Lambda}))/d\sigma(\overline{\Lambda})$ as functions of $p_T^{\rm Breit}$ (a,b) and x_p (c,d) in the target (left) and current (right) regions of the Breit frame. Within the uncertainties, the measurements indicate equal rates of baryon and anti–baryon production.

8 Conclusions

Inclusive K^0_S–mseson and Λ–baryon cross sections have been measured in deep inelastic scattering for $50 < Q^2 < 500\,{\rm GeV}^2$, $3 \cdot 10^{-4} < x < 10^{-1}$, $0.5 < p_T^{K^0_S,\Lambda} < 5\,{\rm GeV}$ and $|\eta^{K^0_S,\Lambda}| < 1.5$. ARIADNE predictions with a strangeness suppression factor of $\lambda_s =$

0.3(0.2) overestimate(underestimate) the total measured cross sections. Also the ratio of the total Λ to K_S^0 cross section is reasonably well simulated by ARIADNE. The HERWIG prediction underestimates the K_S^0 cross section and overestimates the Λ cross section.

The Monte Carlo models do not describe well the ratio of Λ to K_S^0 production in the low p_T region and in the forward region. In general, HERWIG does not reproduce the shape of the K_S^0 and Λ differential cross sections. The data may indicate an increasing strangeness suppression factor with increasing p_T^{Breit} and x_p, in the target region of the Breit frame. The measurements show an equal production of Λ and $\overline{\Lambda}$ as functions of p_T^{Breit} and x_p.

References

[1] B. Andersson et al., Phys. Rep. **97**, 31 (1983).

[2] OPAL Coll., P.D. Acton et al., Z. Phys. **C 56**, 521 (1992);
OPAL Coll., R. Akers et al., Z.Phys. **C 68**, 1 (1995);
ALEPH Coll., D. Buskulic et al., Z.Phys. **C 69**, 379 (1996);
DELPHI Coll., P. Abreu et al., Z.Phys. **C 73**, 61 (1996).

[3] OPAL Coll., G. Abbiendi et al., Eur. Phys. J. **C**, 407 (2000).

[4] SLD Coll., K. Abe et al., Phys. Rev. **D 59**, 052001 (1999).

[5] ZEUS Coll., M. Derrick et al., Z. Phys. **C 68**, 29 (1995);
H1 Coll., S. Aid et al., Nucl. Phys. **B 480**, 3 (1996);
ZEUS Coll., S. Chekanov et al., Phys. Lett. **B 553**, 141 (2003).

[6] H1 Coll., C. Adloff et al., Z. Phys. **C 76**, 213 (1997).

[7] ZEUS Coll., U. Holm (ed.), *The ZEUS Detector*. Status Report (unpublished), DESY (1993), available on `http://www-zeus.desy.de/bluebook/bluebook.html`.

[8] N. Harnew et al., Nucl. Inst. Meth. **A 279**, 290 (1989);
B. Foster et al., Nucl. Phys. Proc. Suppl. **B 32**, 181 (1993);
B. Foster et al., Nucl. Inst. Meth. **A 338**, 254 (1994).

[9] M. Derrick et al., Nucl. Inst. Meth. **A 309**, 77 (1991);
A. Andresen et al., Nucl. Inst. Meth. **A 309**, 101 (1991);
A. Caldwell et al., Nucl. Inst. Meth. **A 321**, 356 (1992);
A. Bernstein et al., Nucl. Inst. Meth. **A 336**, 23 (1993).

[10] H. Abramowicz, A. Caldwell and R. Sinkus, Nucl. Inst. Meth. **A 365**, 508 (1995).

[11] S. Bentvelsen, J. Engelen and P. Kooijman, *Proc. Workshop on Physics at HERA*, W. Buchmüller and G. Ingelman (eds.), Vol. 1, p. 23. Hamburg, Germany, DESY (1992).

[12] K.C. Höger, *Proc. Workshop on Physics at HERA*, W. Buchmüller and G. Ingelman (eds.), Vol. 1, p. 43. Hamburg, Germany, DESY (1992).

[13] F. Jacquet and A. Blondel, *Proceedings of the Study for an ep Facility for Europe*, U. Amaldi (ed.), p. 391. Hamburg, Germany (1979). Also in preprint DESY 79/48.

[14] ZEUS Coll., S. Chekanov et al., Eur. Phys. J. **C 21**, 443 (2001).

[15] A. Bamberger et al., Nucl. Inst. Meth. **A 382**, 419 (1996).

[16] G. Marchesini et al., Comp. Phys. Comm. **67**, 465 (1992).

[17] L. Lönnblad, Comp. Phys. Comm. **71**, 15 (1992).

[18] B. Anderssen, G. Gustavson, L. Lönnblad, U. Petterson, Z.Phys. **C 43**, 625 (1989).

[19] H.L. Lai et al., Phys. Rev. **D 51**, 4763 (1995).

[20] T. Sjöstrand, PYTHIA 5.7 AND JETSET 7.4 PHYSICS AND MANUAL, 1993. Preprint CERN-TH 7112/93.

[21] B. R. Webber, Nucl. Phys. **B 238**, 492 (1984).

[22] H. Spiesberger, HERACLES *and* DJANGOH*: Event Generation for ep Interactions at HERA Including Radiative Processes*, 1998, available on `http://www.desy.de/~hspiesb/djangoh.html`.

[23] Particle Data Group, D.E. Groom et al., Eur. Phys. J. **C 15**, 1 (2000).

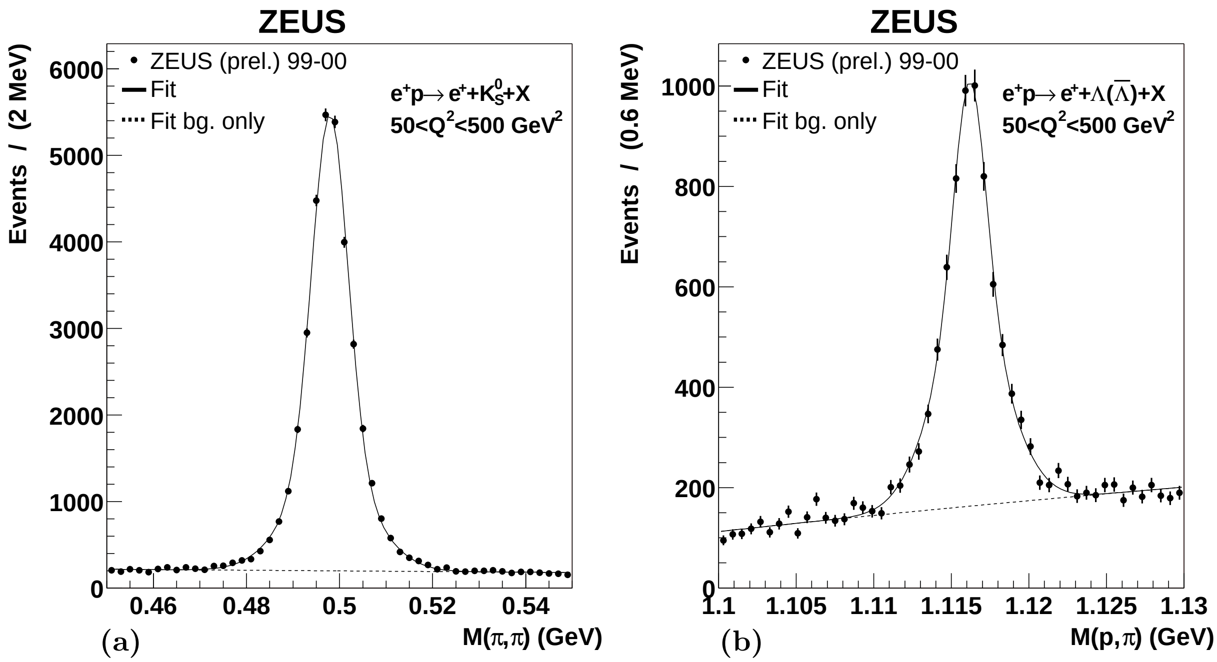

Figure 1: *Invariant mass of K_S^0 (a) and Λ (b) candidates (points with statistical error bars) in the restricted kinematic region as described in the text. The solid line, fit with two Gaussian distributions plus a background term, shows the result. The dashed line shows only the background term of the fit.*

	ZEUS (prel.)	CDM: λ_s=0.3	CDM: λ_s=0.2	HERWIG
$\sigma(K_S^0)$ [pb]	$2454 \pm 18^{+32}_{-102}$	2762	2257	1854
$\sigma(\Lambda+\bar{\Lambda})$ [pb]	$567 \pm 12^{+13}_{-34}$	603	483	1329
$\sigma(\Lambda)$ [pb]	$292 \pm 9^{+7}_{-18}$	302	240	661
$\sigma(\bar{\Lambda})$ [pb]	$279 \pm 9^{+12}_{-18}$	301	243	668
$\sigma(\Lambda+\bar{\Lambda})/\sigma(K_S^0)$	$0.231 \pm 0.005^{+0.005}_{-0.006}$	0.218	0.214	0.717
$\sigma(\Lambda)/\sigma(\bar{\Lambda})$	$1.05 \pm 0.05^{+0.05}_{-0.05}$	1.00	0.99	0.99

Table 1: *Total K_S^0 and Λ cross sections compared to ARIADNE (CDM) and HERWIG. The ARIADNE predictions are shown for $\lambda_s = 0.2$ and $\lambda_s = 0.3$.*

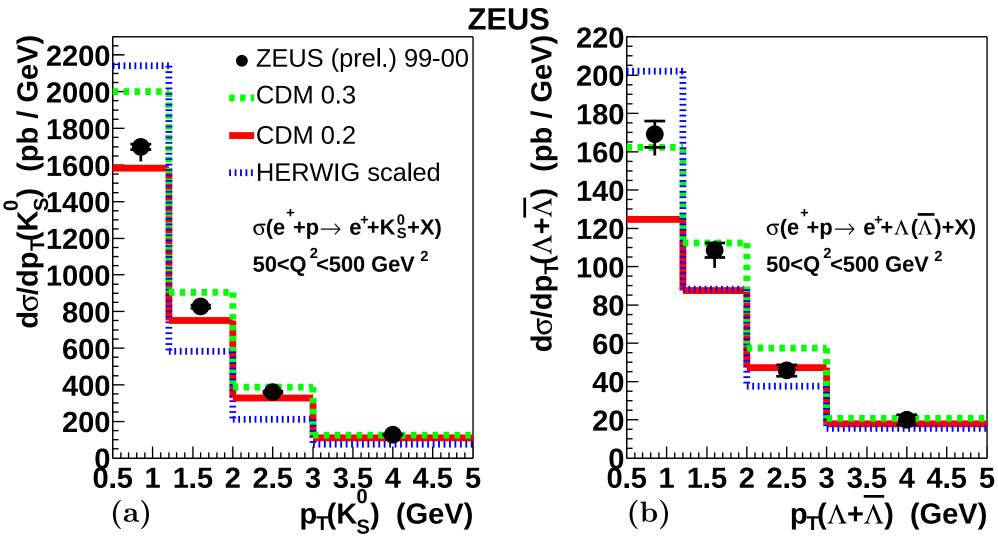

Figure 2: *Differential K_S^0 (a) and Λ (b) cross sections as functions of p_T, compared to ARIADNE (CDM) and HERWIG. The ARIADNE predictions are shown for $\lambda_s = 0.2$ and $\lambda_s = 0.3$. The HERWIG predictions are scaled to the area below the data in each distribution. The inner error bars show the statistical uncertainties, and the outer error bars, the statistical and systematic uncertainties added in quadrature.*

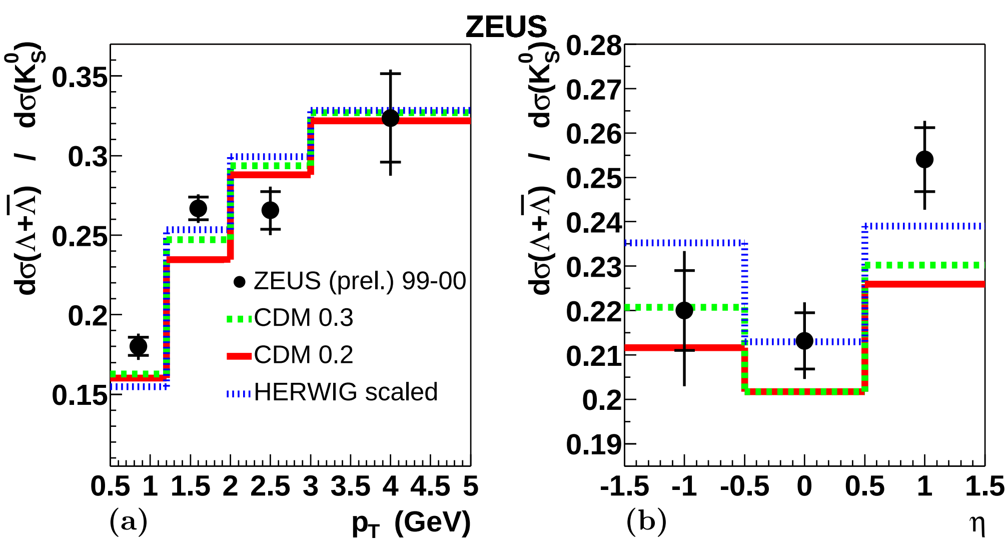

Figure 3: *Differential ratios $d\sigma(\Lambda)/d\sigma(K_S^0)$ as functions of p_T (a) and η (b), compared to ARIADNE (CDM) and HERWIG. The ARIADNE predictions are shown for $\lambda_s = 0.2$ and $\lambda_s = 0.3$. The HERWIG p_T and η predictions are scaled by 0.28 and 0.32, respectively. The inner error bars show the statistical uncertainties, and the outer error bars, the statistical and systematic uncertainties added in quadrature.*

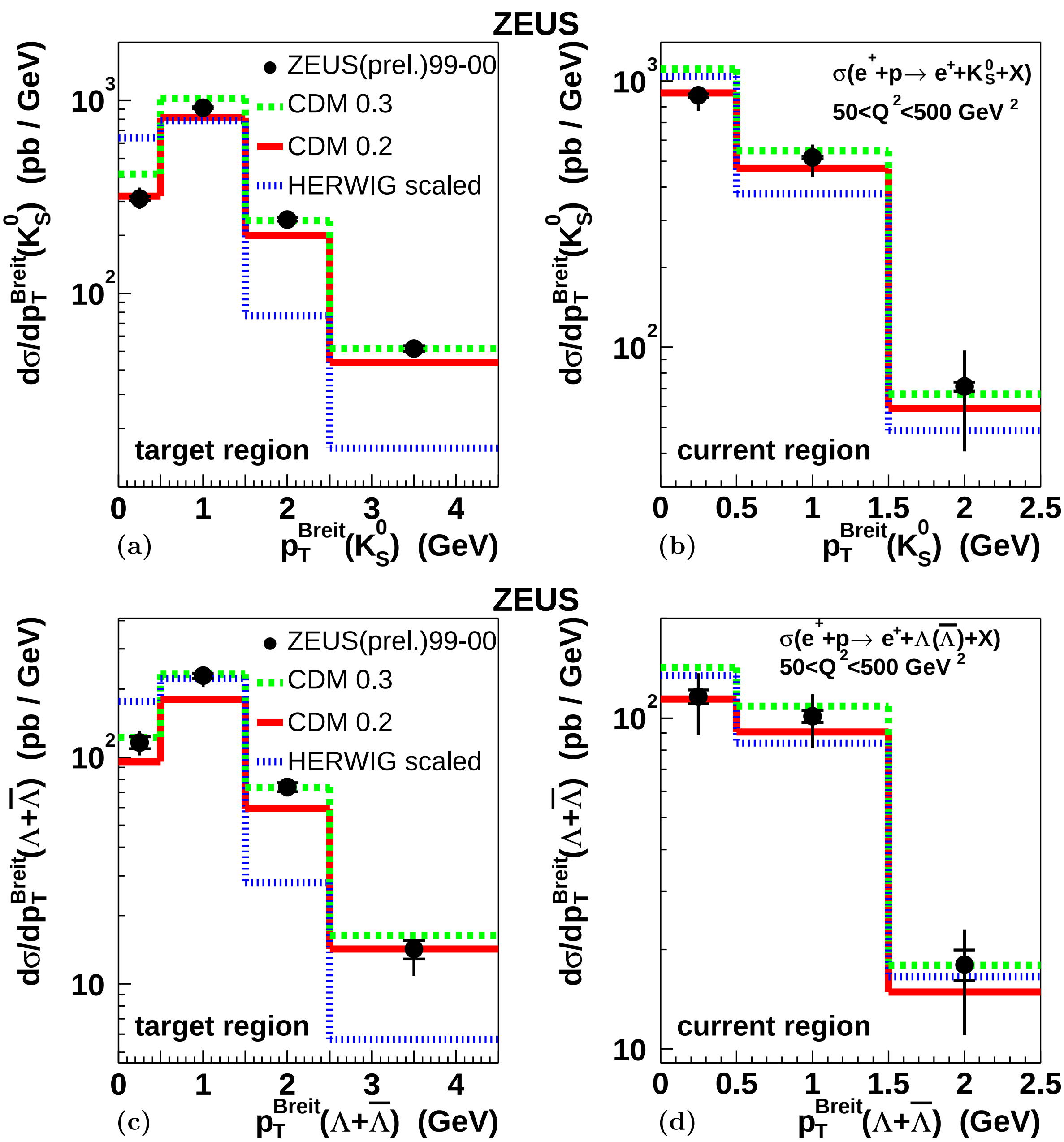

Figure 4: *Differential K_S^0 (a,b) and Λ (c,d) cross sections as functions of p_T^{Breit} in the target and current regions of the Breit frame, compared to ARIADNE (CDM) and HERWIG. ARIADNE predictions are shown for $\lambda_s = 0.2$ and $\lambda_s = 0.3$. The HERWIG predictions are scaled to the area below the data in each distribution. The inner error bars show the statistical uncertainties, and the outer error bars, the statistical and systematic uncertainties added in quadrature.*

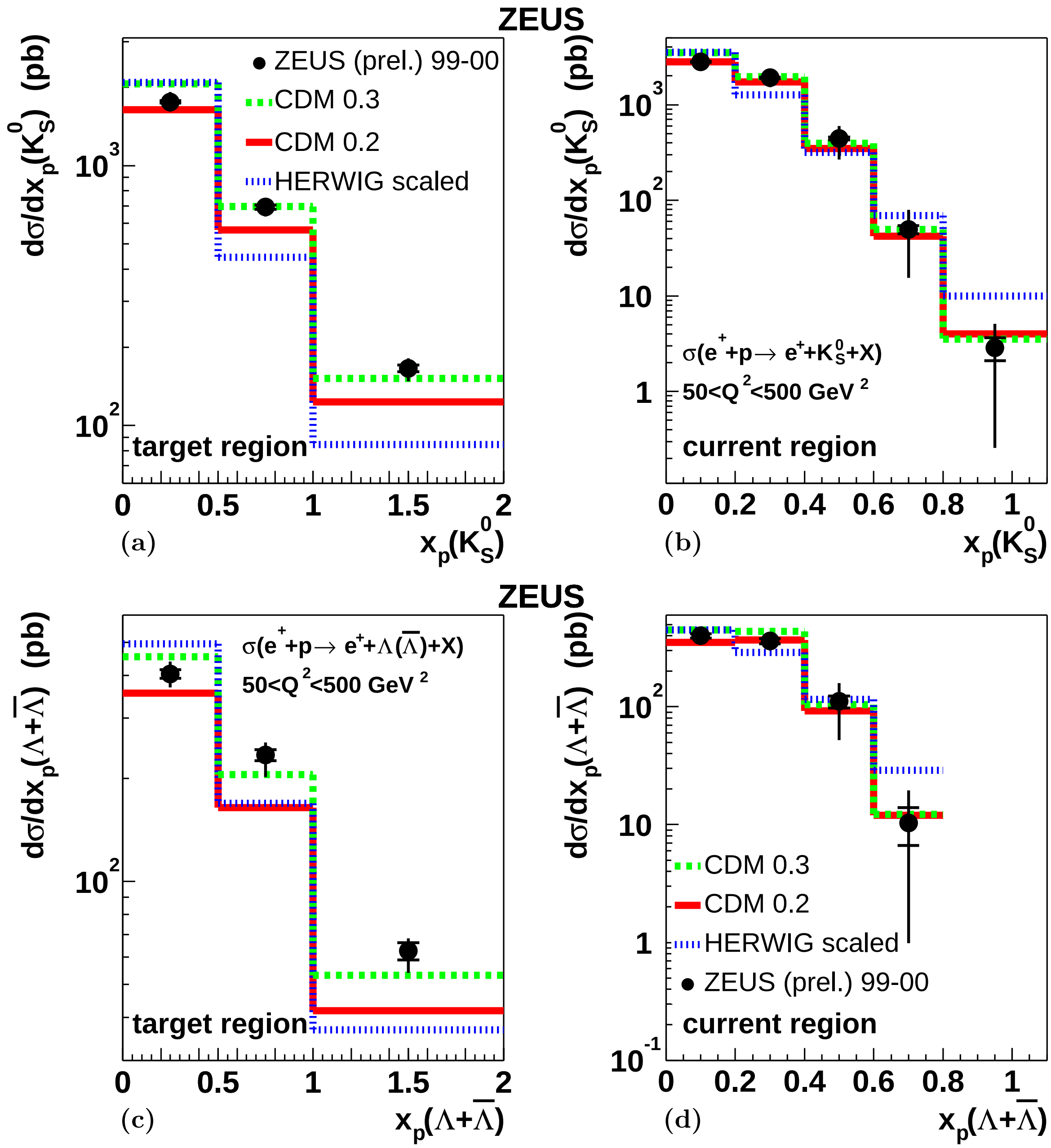

Figure 5: *Differential K^0_S (a,b) and Λ (c,d) cross sections as functions of x_p in the target and current regions of the Breit frame, compared to ARIADNE (CDM) and HERWIG. The ARIADNE predictions are shown for $\lambda_s = 0.2$ and $\lambda_s = 0.3$. The HERWIG predictions are scaled to the area below the data in each distribution. The inner error bars show the statistical uncertainties, and the outer error bars, the statistical and systematic uncertainties added in quadrature.*

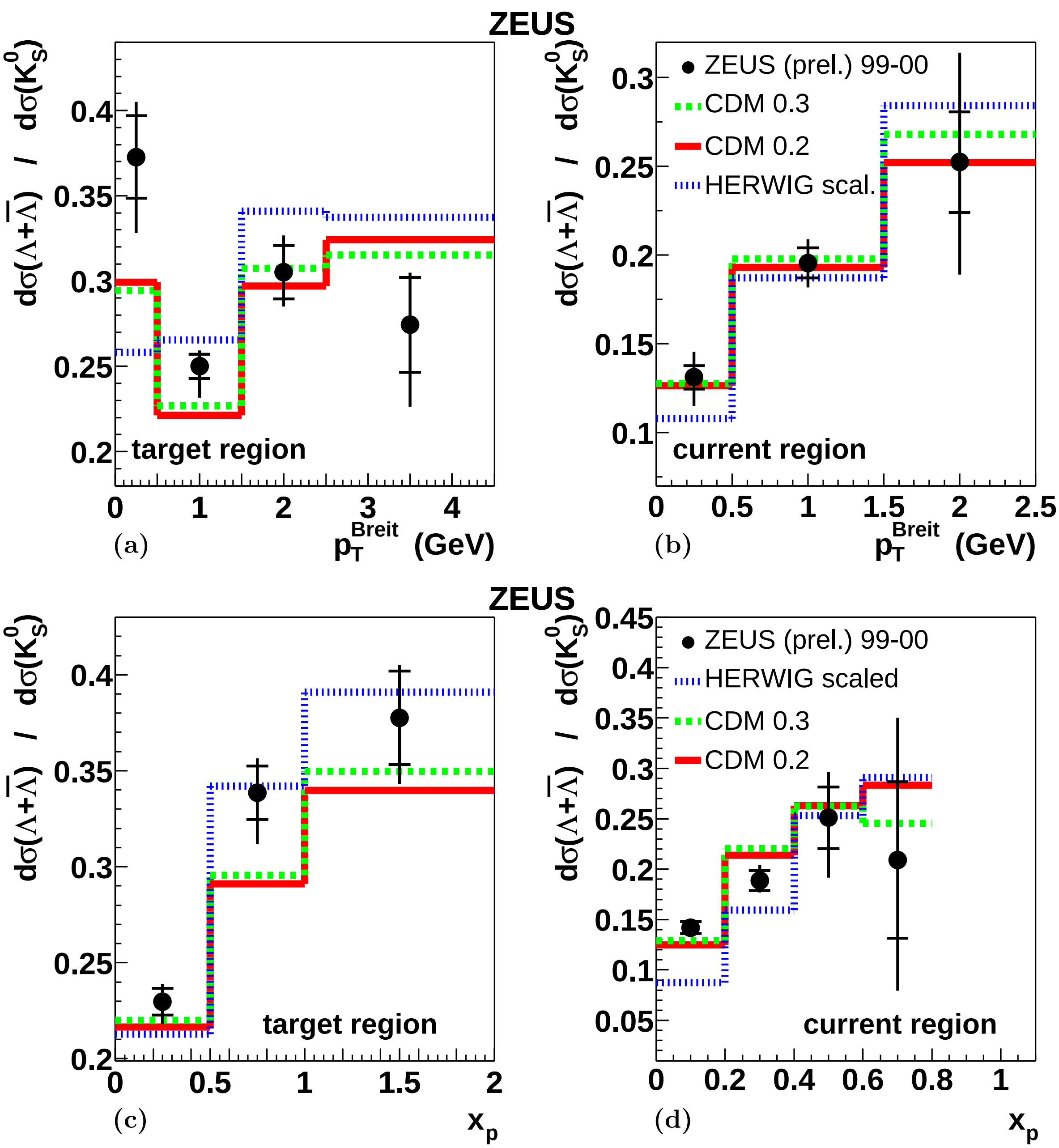

Figure 6: *Differential ratio $d\sigma(\Lambda)/d\sigma(K^0_S)$ as functions of $p_T^{\rm Breit}$ (a,b) and x_p (c,d) in the target and current regions of the Breit frame, compared to ARIADNE (CDM) and HERWIG. The ARIADNE predictions are shown for $\lambda_s = 0.2$ and $\lambda_s = 0.3$. The HERWIG predictions are scaled by 0.31, 0.28, 0.28 and 0.45 in a), b), c) and d), respectively. The inner error bars show the statistical uncertainties, and the outer error bars, the statistical and systematic uncertainties added in quadrature.*

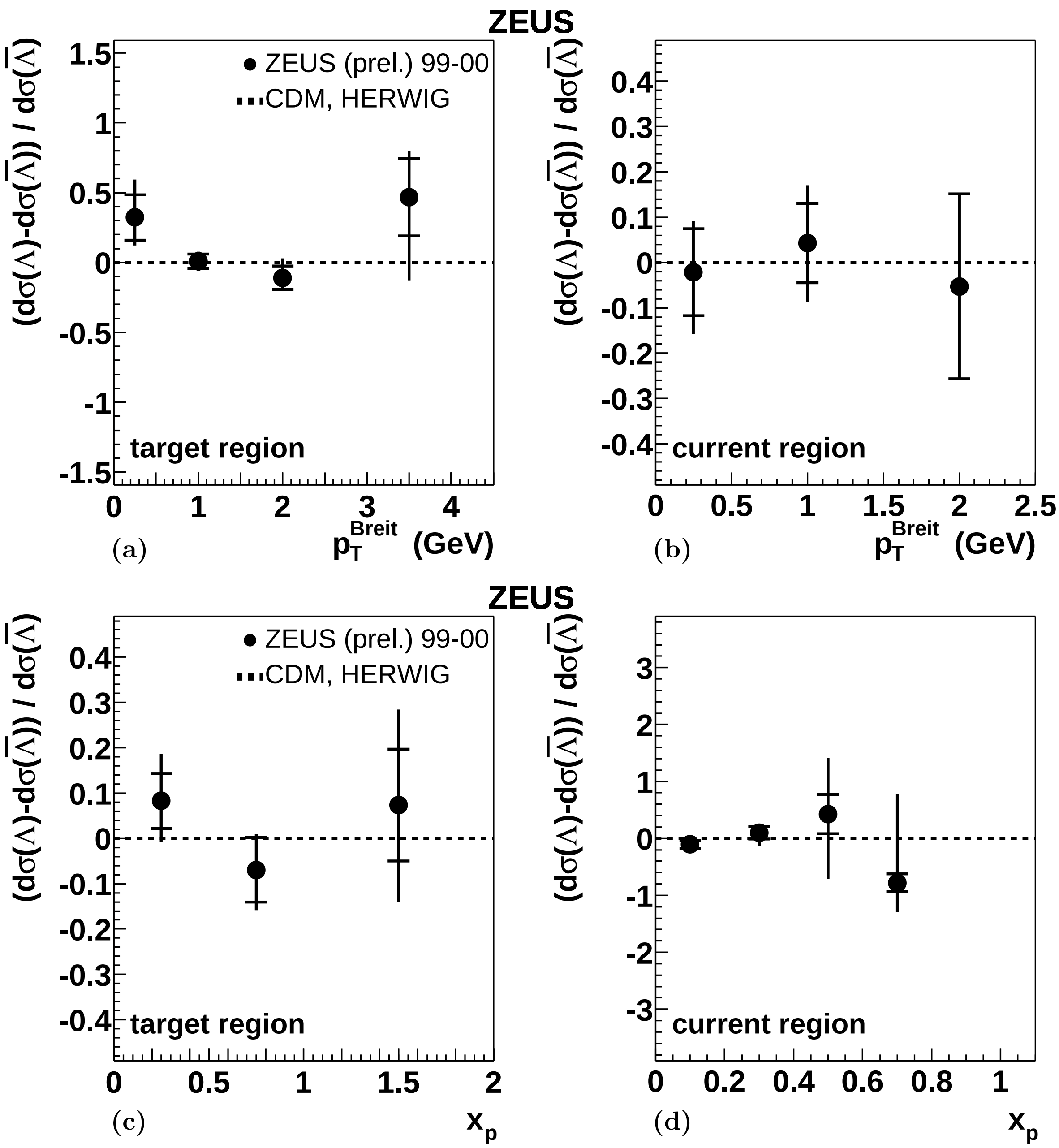

Figure 7: *Ratio* $(d\sigma(\Lambda)-d\sigma(\bar{\Lambda}))/d\sigma(\bar{\Lambda})$ *as functions of* p_T^{Breit} *(a,b) and* x_p *(c,d) in the target and current regions of the Breit frame, compared to ARIADNE (CDM) and HERWIG. The inner error bars show the statistical uncertainties, and the outer error bars, the statistical and systematic uncertainties added in quadrature.*